DISINTEGRATING PAPER-BASED TOUCH SENSORS

By

JIHYUN RYU

A thesis submitted to the

Graduate School-New Brunswick

Rutgers, The State University of New Jersey

In partial fulfillment of the requirements

For the degree of

Master of Science

Graduate Program in Mechanical and Aerospace Engineering

Written under the direction of

Aaron Mazzeo

And approved by

_____

_____

_____

New Brunswick, New Jersey

May, 2016

ABSTRACT OF THE THESIS

DISINTEGRATING PAPER-BASED TOUCH SENSORS

By JIHYUN RYU

Thesis Director:

Professor Aaron Mazzeo

This thesis investigates the disintegrating properties of compacted cellulose-based material used as touch sensors. Pressurized compaction of powdered microcrystalline cellulose (MCC) enabled the fabrication of compacted substrates with quantities ranging from 50 mg to 400 mg and with pressure from 45 to 135 MPa. Along with the quantity of powdered MCC and compressive pressure, thin sheets had thicknesses varying from 190 to 1210 μm and porosities ranging from 19% to 47%. With agitated flows of bubbles of 2.7 $cm^3/_{sec}$ to speed up the rate of transiency, the cross-sectional area of the substrates disintegrated by 89% to 100% in approximately an hour. The area of the substrate was plotted as a function of time on a logarithmic scale to describe the transient, disintegrating behavior. The rate of disintegration was related to the degree of porosity and thickness of the substrates, according to dimensional analysis. Touch sensors fabricated with stencil-patterned electrodes made suitable platforms for other electronic components, tested with a microprocessor-based system.

ACKNOWLEDGMENT

It is my great pleasure to express my deep sense of gratitude to my advisor Dr. Aaron Mazzeo, it is him who guided me, encouraged me to keep working on the transient touch sensor. I am very grateful for his advice, ideas and guidance, which have been of crucial importance to this work. He offered me an absolute freedom and ample opportunities that gave me inspirations.

To Sandesh Gopinath, Jingjin Xie, and all other lab mates, thank you for all your help and support. Your support has been unwavering and very much appreciated. They also offered me ideas and inspirations, as well as both of you tried to create such a nice atmosphere in doing the research.

The seniors and undergraduate students who shared their knowledge and wisdom with me, among others, I would like to mention Adrian Rodriguez, Deanna Ko, and Sean Wu.

DEDICATION

This dissertation is gratefully dedicated to my beloved parents and my sister.

I also appreciate the dedication of all those who have contributed to discussions and made corrections: David Sejin Park, Monica Lee, Kyung Chan Kim, Jake Taewan Kim, Sophie Chen, and Khadija Mohamed.

Table of Contents

List of Figures

1. Introduction

The growing demand for electronics has led to shorten service life of devices, which has resulted in high levels of a waste stream, known as "E-waste" [1]. Conventional metallic and plastic electronic devices or components designed to be stable and widely used are generally non-renewable or non-degradable, which can potentially cause adverse environmental impacts as they often contain toxic materials such as gallium arsenide and cadmium[1][2]. New technologies in the subfield of degradable electronics[3] have demonstrated capabilities for complete dissolution in quiescent liquids[4][5].

Hwang, et al. focused on the modeling/fabrication of transient electronic substrates which dissolved in quiescent bodies of water[5]. The "vanishing" nature of transient electronic devices in quiescent liquids ranged from minutes to days depending on the composition of the substrate[5][6]. However, there are still open questions about modeling and characterizing the dissolution or disintegration of transient electronic devices in agitated flows of solvent. There are opportunities to reduce the cost and complexity of materials and processes used for the fabrication of electronic devices with the use of environmentally sustainable materials, such as paper-based or polymer-based materials[7][8][9]. Such cellulose-based materials are receiving attention as potentially versatile, cost-effective electronic devices and sensors. These renewable materials refined from trees or plants may be suitable as substrates for the manufacture of low-cost, simple, and efficient electronic components.

Powdered microcrystalline cellulose (MCC), often utilized in pharmaceutical tablets as a binding material, has configurations of regularly repeating cellulose polymer chains that are stable when exposed to moisture[10][11]. While not soluble in water,

compacted MCC will disintegrate or separate into microscopic particles with agitation. Many experiments have used a rotating paddle in a container with standardized geometries to characterize the disintegration of compacted tablets. As the rotating speed of a shaft increases, the flow shortens the time to disintegrate the substrates[12]. For MCC compacted at a pressure higher than 80 MPa, it can take more than an hour to disintegrate completely in a container with a mixing flow[13]. Nonetheless, substrates for electronic applications will likely require distinct aspect ratios with thin sheets instead of thick tablets, and there appears to be a lack of information in the literature concerning the disintegration of thin sheets of compacted MCC.

The overarching goal of this work is to understand how agitation affects the rate of disintegration of cellulose-based substrates suitable for transient electronic applications. The use of mechanically agitated solutions with bubbly flows enhances the mixing performance and the disintegration of substrates. As expected, the above process successfully degrades transient electronic devices at faster rates than in quiescent flows. This work also presents the Buckingham-Pi Theorem-based dimensional analysis to address the scalability of the approach.

Since cellulose-based substrates behave as insulators (i.e., resistance to flow of electric charges), a conductive material was printed on the substrates to build paper-based circuits. Conductive paint (Bare Paint) is an inexpensive, non-toxic material that quickly dries at room temperature. It is also compatible with many surfaces including paper, plastic, and fabrics. In this work, we employed this conductive ink to pattern electrical traces without soldering on the cellulosic substrates. The electrical traces handled low-current electrical signals with potentials between 0 and 5 Volts.

2. Experimental Design

The fabrication and characterization of a transient touch sensor required multiple experimental steps: pressurized compaction, mechanical agitation, stencil-based patterning of conductive traces, and testing with an Arduino-based system. Pressurized compaction was the method used for the fabrication of a thin sheet from a powder. Mechanical agitation with a bubbly flow facilitated disintegration of substrates. Stencil-based patterning applied conductive ink that served as electrical circuitry on the surface of the insulating compacted MCC. The Arduino-based system served as the electronic system for detecting touch.

2.1. Compaction of Microcrystalline Cellulose

Direct compression is the key mechanism employed to fabricate thin transient substrates for electronic touch sensors. This manufacturing process is simple and similar to conventional techniques for tableting, which enable the mass production of tablets with desired uniformity. For the pressurized compaction, we initially constructed a punch tool made of steel. Turning a metallic rod in a lathe, we fabricated a flat-faced punch with a diameter of 19.0 mm (i.e., 0.75 inches). To machine a die cavity with a thickness of 3.5 cm, we drilled a hole cut through the center of a metallic plate to match the punch. The punch and die system formed a thin sheet by localizing the applied pressure with a small clearance which restricted the radial expansion of the powder. For pressurized compaction, we started with placing a specified mass of powdered MCC in the oven under the temperature of 50 ºC for 30 minutes to evaporate the moisture and limit the variable effects from humidity. The dried powder was manually fed into the enclosed cavity of the die.

Figure 1a describes the initial volume occupied by the un-compacted powdered MCC was greater than the compacted volume of the discrete particles. A manual hydraulic press (Carver Lab Press) provided compressive pressure to compact the powdered MCC to a thin sheet. The punch dwelled in the die for 30 seconds. During the compaction, the compressive pressure plastically deformed the powdered MCC and increased the area of internal bonding. Hence, the plastic deformation caused the reduction in the volume of pores between the discrete particles as illustrated in Figure 1b. Figure 1c shows a thin sheet fabricated with 200 mg at 90 MPa with a diameter of 19.0 mm (i.e., 0.75 inches).

The difference in the amount of powdered MCC used for pressurized compaction resulted in a varying range of thicknesses for the thin sheets. In ascending order of mass from 50 mg to 400 mg (i.e., 50 mg, 100 mg, 200 mg, and 400 mg), the thicknesses of thin sheets showed the pressure dependent tendency. Varying the compressive pressure ranging from 45 MPa to 135 MPa (i.e., 45 MPa, 90 MPa, and 135 MPa), we set 12 combinations along with the masses and pressures: Combination 1 (50 mg and 45 MPa), Combination 2 (100 mg and 45 MPa), Combination 3 (200 mg and 45 MPa), Combination 4 (400 mg and 45 MPa), Combination 5 (50 mg and 90 MPa), Combination 6 (100 mg and 90 MPa), Combination 7 (200 mg and 90 MPa), Combination 8 (400 mg and 90 MPa), Combination 9 (50mg and 135 MPa), Combination 10 (100mg and 45 MPa), Combination 11 (200mg and 135 MPa), and Combination 12 (400mg and 135 MPa).

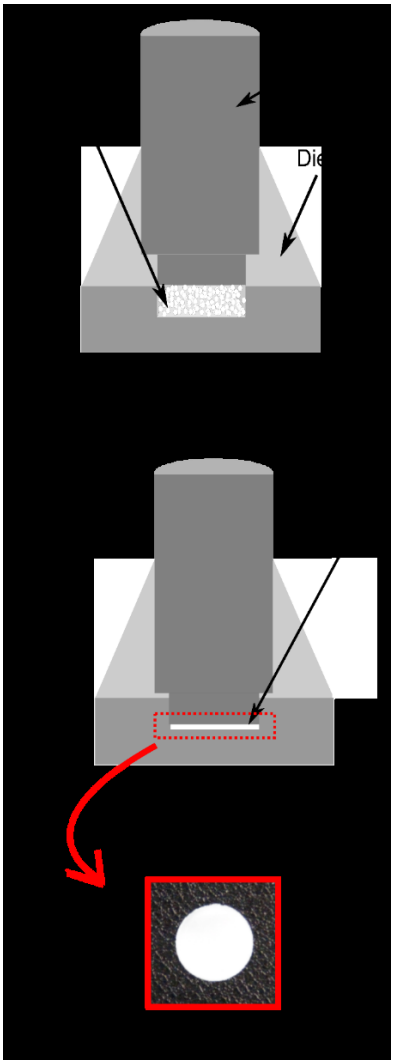

Figure 1: Schematic rendering for direct compression to prepare thin sheets from the powdered MCC using a manual hydraulic press. (a) Initial state for pressurized compaction in the punch and die system with the powder distributed randomly throughout the die mold before the application of compressive pressure. (b) Maintaining the peak pressure to compress the powdered MCC for 30 seconds. (c) Photo of a thin sheet compacted with 200 mg of MCC at 90 MPa which had a diameter of 19 mm and a thickness of 540 µm. The corresponding thicknesses were proportional to the amount of MCC used, while the thicknesses were inversely proportional to applied pressure.

2.2. Platform for Testing the Disintegration of Substrates in Bubbly Flows

As stated above, this work focused on how bubble-agitated water enhanced the rate of disintegration of a transient substrate. To track the changing area of a thin sheet, we first assembled the testing platform. The testing platform consisted of an acrylic box and a cylindrical test area made of sections of syringes with inner diameters of 24.0 mm. A small supporting unit with a mesh screen held the substrate apart from the camcorder (Full HD 60p from Sony) with a distance of 17.0 cm. The unit with mesh screen was removable and placed approximately 3.0 cm away from the top edge of the cylinder and 2.5 cm above the surface of the water. Before gluing the cylinder and acrylic box using epoxy glue and silicone adhesive (Sil-poxy from Smooth-On) to prevent water leakage, we drilled a hole with an outer diameter of 3.20 mm (i.e., 0.13 inches) at a contact surface of the cylinder and acrylic box to connect the air pump and bubble distributor via air tubes. In the middle of the air pump and a bubble distributor, we placed a control valve that allowed the streaming of air flow in one direction.

The system successfully agitated the water with bubbles to disintegrate compacted thin sheets of cellulose and recorded the shrinking cross-sectional areas of the substrates by timed acquisition of still images with the camcorder. To acquire the images, we stopped injecting the air to a bubble distributor for 10 seconds to 1 minute and waited for the water to stagnate before taking a snapshot.

The rate of bubbly flow was proportional to the applied pressure from the air pump. To control the rate of flow, we placed a needle valve (Ultra Precision Needle Valve from Ideal Valve) between the air pump and the air distributor as shown in Figure 2a. We opened

the valve to have an upstream pressure of 17.0 kPa (2.5 psi) and a downstream pressure of 14.0 kPa (2.0 psi). Volumetric flow rate corresponding to the number of turns is

$$Q_G = 962 \times C_v \sqrt{\frac{{P_1}^2 - {P_2}^2}{S.G. \times T}}, \quad (1)$$

where P_1 and P_2 are the upstream and downstream pressures of air in the units of psig, C_v is the flow coefficient of the needle valve with the maximum value of 0.08 in increment of 0.004 for each turn, S.G is the specific gravity of air which has a value of 1.0 where air at 70℉ and 14.7 psia, and T represents the absolute temperature in degrees Rankine.

The number of bubbles varied along with the speed of the bubbles. A high-speed camera (Basler 180km) captured the bubbles that flowed upward in the water at intervals of 0.017 seconds (i.e., 60 fps). During the image processing, a set of recorded images for 30 seconds enabled us to count the number and calculate the volume of bubbles that passed through an arbitrary line. We then converted the volumetric flow rate into a mass flow rate. Tracking bubbles along subsections of test areas at different depths, we made coordinated measurements of the bubbles to ensure the accuracy of the measurements of the average flow rate. With an assumption that the air bubbles were spherical, we used the Ideal Gas Law to describe the relation of gas molecules to their environment through pressure, temperature, and volume:

$$\mathrm{P} \times \mathrm{V} = n \times R \times T, \quad (2)$$

where P is the absolute pressure of air, V is the volume the gas occupies, n is the number of moles of gas present, R is the universal gas constant, and T is the absolute temperature in degrees Kelvin. Because the amount of air in the unit volume represented the density, the expression for the density is obtained by rearranging the Ideal Gas Law

$$\rho = \frac{M \times P}{n \times R \times T}, \quad (3)$$

Knowing the density of air, the product of the density and volumetric flow rate gives the mass flow rate

$$\dot{m} = \rho \times Q, \quad (4)$$

The hydrostatic pressure varies along with the depth from the place of substrate to the bubble distributor can be simply expressed by

$$P = \rho_{water} \times g \times h, \quad (5)$$

where ρ is the density of water at 15 ºC, g is the gravitational acceleration, and h is distance a bubble travels along the graduated cylinder. Substituting the hydrostatic pressure in place of pressure in the Ideal Gas Law, the equation for mass flow rate is

$$\dot{m} = \frac{M \times \rho_{water} \times g \times h}{n \times R \times T} * Q, \quad (6)$$

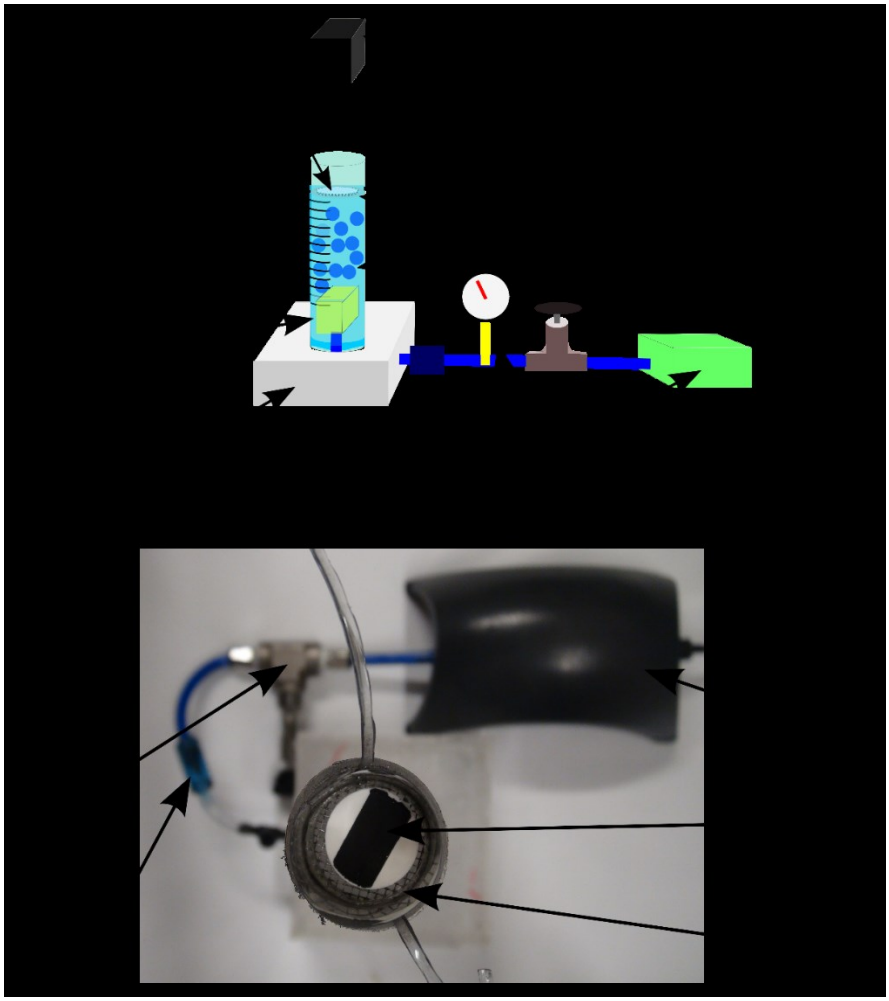

Figure 2: Experimental setup for characterization of the disintegration of a thin sheet of compacted cellulose. (a) Schematic rendering of the platform for the disintegration of a transient substrate in bubble-agitated water. A camera captured the changing areas of transient substrates used for image processing. The needle valve controlled the pressure of the air. (b) Photo of the setup taken by the camcorder from above the experiment. Initially, a thin sheet was placed on the mesh screen approximately 2.5 cm above the surface of the water. After introducing the bubble-agitated water, a thin sheet immersed into the water and bubbles forcibly broke apart a substrate and then disintegrated residue sunk to the bottom when they were small enough to pass through the mesh screen.

2.3. Printing of Conductive Traces on a Substrate

A cellulose-based material derived from wood pulp is an electrically resistive material which forms the substrate. A dielectric constant is an index which describes the ability of a capacitor to store charges[14]. For the measurement of a dielectric constant for the compacted substrates, we applied the conductive ink on both surface of a thin sheet to make a parallel-plate capacitor containing a dielectric that filled the voids between the surfaces. The dielectric constant, denoted by ε_r, is calculated by

$$\varepsilon_r = \frac{C \times d}{A \times \varepsilon_0}, \tag{7}$$

where C is the capacitance of a thin sheet, d is the thickness of a substrate, A is the area of surface, and ε_0 is a permittivity of air (i.e., $8.854*10^{-12}$ F/m).

The substrate is further patterned with conductive electrodes to create a touch sensor. Patterning the electrode, as demonstrated step by step in Figure 3, involves masking the compacted MCC with a stencil pattern[15] and applying the conductive ink to the opened areas rendered by stencil. A laser engraver (VersaLaser from Universal Laser Systems) is used to cut the desired pattern in the stencil with the dimensions of 11 mm width and 17 mm height on a self-adhering film (Frisket Film), then attached it to the substrate as illustrated in Figure 3a. To secure the attachment of film and substrate, we gently rubbed and tapped the portion of contacting area with a tip of a blunt object. Figure 3b represented that the use of a squeegee allowed spreading of the uniform thickness of conductive material along the open mask to accommodate a desired trace of electrodes on the compacted thin sheet. To keep substrates away from the humidity and increase the rate of drying, we placed the substrates in the plastic container for 15 min keeping them at room

temperature. After the conductive ink was sufficiently dried, we carefully removed the film as depicted in Figure 3c. The thin sheet compacted with Combination 7 had a diameter of 19 mm as shown in Figure 3d. The positive and negative charges on each of electrode attracted each other, but the charges coalesced on the electrodes because MCC placed between them.

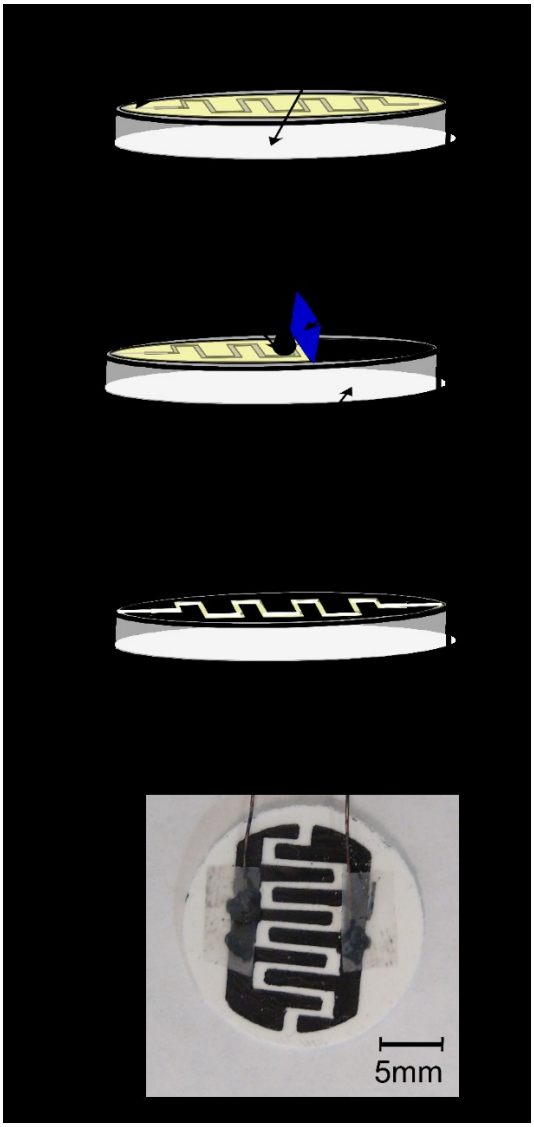

Figure 3: Schematic illustrations of stencil-based method for patterning the electrode on substrate to fabricate of a capacitive button. (a) Laser engraved stencil to create the open pattern on the thin film. The open mask was self-adhesive on the surface of substrate. (b) Throughout the substrate, squeegee uniformly spread the conductive ink along the pattern. (c) After detaching the mask from substrate, a button had E-shaped electrodes composed of conductive ink. A winding path made of the exposed MCC divided electrodes of button. (d) Photo of a single capacitive button. The tape secured the attachment of wires on each electrodes.

2.4. Electrical Characterization and Sensing of Touch

Each button described in this work is a capacitor which has the ability to store an electrical energy. To test the sensing of a touch, we built a simple circuit comprised a capacitive button, resistors, several electronic components, and Arduino-based system. A button connected to the resistor with a value of 330 kΩ and a voltage source in series to have a first order RC circuit (left) allowing to detect a capacitance changed by measuring the impedance when finger bridged the electrical trace as described in Figure 4a (right). The resistor limited the voltage across the capacitor cannot instantly respond to a change in the voltage source. Arduino Uno generated the step input of 5V to RC circuit and detected how much time the capacitive button took to charge, giving it an estimate of the capacitance[16]. An integrated circuit (IC) combined with the RC circuit was a voltage amplifying device, the operational amplifier (op-amp). The difference between the input and output impedances determined the gain of the op-amp. By taming the high differential voltage, the output signal is in-phase with the signal of entry, and then the non-inverting operational circuit produced a unity gain. To buffer the output signal when a finger touched a button that flowed into the RC circuit, we used an operational amplifier (μa741) to build the voltage follower. Figure 4b depicted the simple circuit for the sensing of touch. Digital input pins of Arduino UNO only offered two possible states, which were on or off. A finger triggered the circuit with some impedance as described by the paper on paper-based touch pads[7]. When a finger bridged the gap between the active electrode and grounded electrode, the Arduino-based system detected the changes in capacitance, then lit up the light emitting diode (LED).

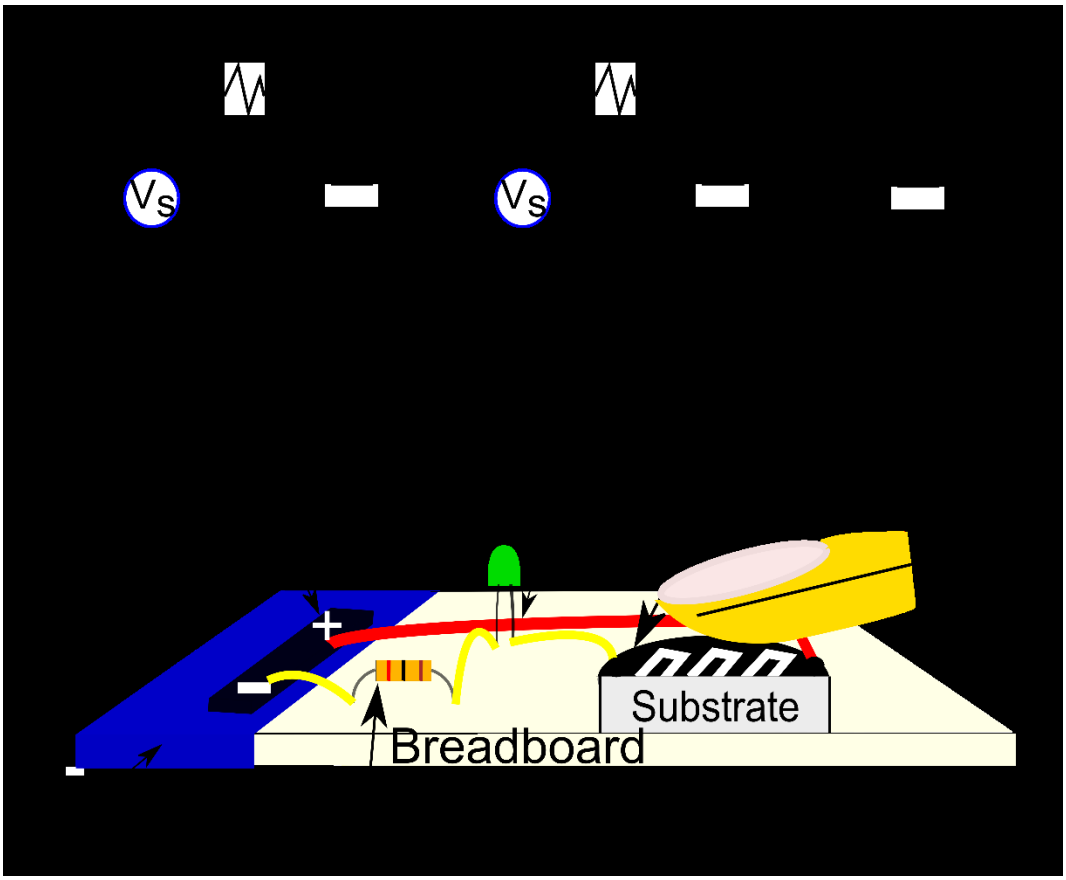

Figure 4: Schematic drawing for sensing of touch of a single button that formed the RC circuit. (a) Description of an ideal RC circuit without (left) and with (right) external coupling of the finger. Since human body contains the water act as electrolytes which caused the change the capacitance in the RC circuit when finger touched a capacitive button. (b) Arduino UNO lit up the LED by estimating the time to charge the button when finger bridged the active and ground electrodes.

2.5. Characterization of Disintegration of Substrate

For the scale of transience, the observations of the changing area as a function of time explain how bubbles enhanced the disintegration of the individual thin sheet, fabricated with different experimental combinations. Each set of combinations consisted of twenty consecutive images taken by the camcorder during the assigned time domain ranging from 0.5 seconds to 1 hour in a logarithmic scale; then the images were evaluated to track the change in the size of compacted thin sheet. MATLAB Image Processing Toolbox detected the size reduction of a thin sheet remained on the mesh screen and eliminated the undesired segments that caused the error in calculation of the area of substrate. For example, the script for morphological enhancement and analysis techniques removed a mesh screen placed beyond of the substrate and reflection of light on the surface of water in the object processing.

Based on the changing area as a function of time, increasing the compaction pressure brought the particles closer to each other that caused a decrease in the degree of porosity. A thin sheet compacted with Combination 12, in turn, had the lowest porosity, resulting in the slowest speed of the disintegration of the 12 combinations. Through the dimensionless analysis, we made the expectation of the behavior of a system, including the parameters that affected the rate of the disintegration of transient substrates with a limited number of experiments. The basic theorem of non-dimensional analysis supported the effect of porosity using the relationship between the physical quantities and the magnitudes of the base units to derive the logical consequences. The Buckingham Pi theorem simplified a physical problem by appealing to dimensional homogeneity that enabled the limited

number of dimensionless Π parameters to acquire the propensity of the disintegration in the water.

3. Results and Discussion

Regarding the disintegrating touch sensor, this section refers to the aspect of disintegration of transient substrate and performance of electrical touch sensor/ keypad: the transient behavior as a degradable substrate in the bubble-agitated water and the functionality as an electrical touch sensor.

3.1 Disintegration of Transient Substrate

As a consequence of the densification of powdered MCC, the quantity of powdered MCC varied the resulting thicknesses of transient substrates. The use of a micrometer (Anytime Tools) enabled the measurement of the thickness of each combination. We measured the thickness at five points (i.e., center, top, bottom, left, and right), used to calculate the degree of pore structure in thin sheets. Since the die cavity limited the radial expansion, the thickness is the only concern, closely associated in the porous structure of a thin sheet. The porosity of MCC played a major role in the calculation of volume. The equation for the porosity was simply defined as a ratio of bulk to true density of the thin sheet. The porosity was inversely proportional to bulk density complied with thickness of the substrate

$$Porosity = 1 - \frac{\rho_{bulk}}{\rho_{true}}, \quad (8)$$

The value for theoretical true density of powdered MCC is 1.60 $^{g}/_{cm^3}$ [16] which had a constant value at room temperature, while the thickness of a tablet varied correspondingly to the experimental conditions of compression. Consequently, a given quantity of MCC compressed at different pressure, thinner substrates have the higher density. Combinations 1 through 4 fabricated with the compressive pressure of 45 MPa had resulting thicknesses of 210 μm, 350 μm, 640 μm, and 1210 μm, and their corresponding porosities were 47%, 37%, 32%, and 28 %, respectively. At the pressure of 90 MPa, the thicknesses of Combinations 5 to 8 were 200 μm, 310 μm, 610 μm, and 1130 μm while their porosities were 45%, 30%, 28%, and 22 %, respectively. For the remaining four combinations with 135 MPa, the thicknesses were 190 μm, 300 μm, 570 μm, and 1080 μm, porosities were 43%, 30%, 23%, and 19 %, respectively. This differences was used for tracking the area changing in the bubble-agitated water. Thin sheets produced with 12 combinations, the thicknesses were inversely proportional to the degree of porosities.

Each experiment for the disintegrating 12 combinations was conducted two times in the bubble-agitated water to increase the accuracy of image processing; then we averaged each set of data to identify the difference in the rate of disintegration regarding the change in the degree of porosity. The wide range of thickness domain and the level of porosity for compacted MCC, therefore, had significant impact on the rate of disintegration. With given restrictions varying the compressive pressure and the mass of powder for compaction of cellulosic powder, porosities, which affected the speed of the disintegration, complied with the thickness of the substrate. The bubble distributor controlled by the needle valve provided the bubbly flow with the volumetric flow rate of 2.7 $^{cm^3}/_{sec}$ (i.e., 0.08 mg/sec). Figure 5 showed five serial images that captured the

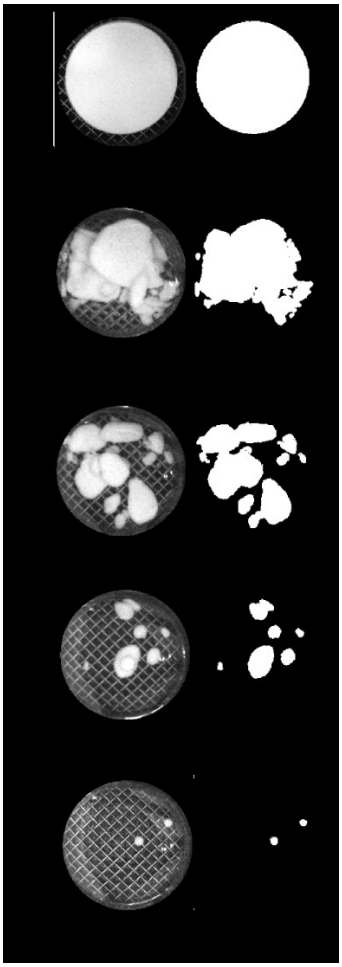

Figure 5: A set of five images demonstrated the disintegration of a transient substrate in the bubble-agitated water with the volumetric flow rate of $2.7 \mathrm{cm}^3 / \mathrm{sec}$. *To facilitate visualization, the contrast adjusted images (left) were juxtaposed with the post-processed images (right). The script used in image processing detected an outline of the disintegrating substrate, and then calculated the area of residues on the mesh screen. (a) Before introducing the bubbly flow, a thin sheet was placed on the mesh screen. (b) After 5.5 seconds, bubbles broke the substrate into several chunks of particle. (c) Air drastically reduced the size of a compacted MCC in 48 seconds. (d) For about 10 minutes, agitated water disintegrated more than half of the transient substrate. (e) Only a few particles remained on the mesh after 1 hour.*

changing area of a transient substrate at different times and their corresponding post-processed images. The MATLAB script converted the contours of a particles remained on the mesh screen into the post-processed images. The bubble-agitated water gradually disintegrated Combination 7, as a consequence, the introduced bubbles degraded 30%, 48%, 89%, and 99 % of the initial size of a thin sheet after 5.5 seconds, 48 seconds, 630 seconds, and 1 hour, respectively. This tendency of size reduction of transient substrates in bubbly flow also emerged from the other 11 combinations.

Figure 6 illustrates the effectiveness of bubble-agitated water on the rate of disintegration of thin sheets. Along with the techniques of image processing for the calculation of the changing area, it was possible to make a comparison between with and without bubbly flow from the semi-log plot of which represented the size of particles remained on the mesh screen as a function of logarithmic time. When the water contacted with the compacted MCC, the molecules of the water weaken the intermolecular bonds by moving away from each other. As compacted thin sheets absorbed the water, it subsequently swelled rather than dissolving or disintegrating by contacting with the water. As a result, the areas of the substrates grew and the cracks appeared on the surface.

The area of a substrate in the bubbly flow decreased sharply corresponding to the quantity of powdered MCC used and the degree of porosity. The efficacy of bubbles in the disintegration of compacted substrates was analyzed by comparing the changing area of a thin sheet in the bubble-agitated to in the quiescent water. Under the given volumetric flow rate of 2.7 $cm^3/_{sec}$ for all 12 combinations, the bubbly flow degraded half of the thin sheet in five minutes, while the remaining residues required a longer time to be broken apart since the beginning stage of disintegrating test had a higher possibility for the

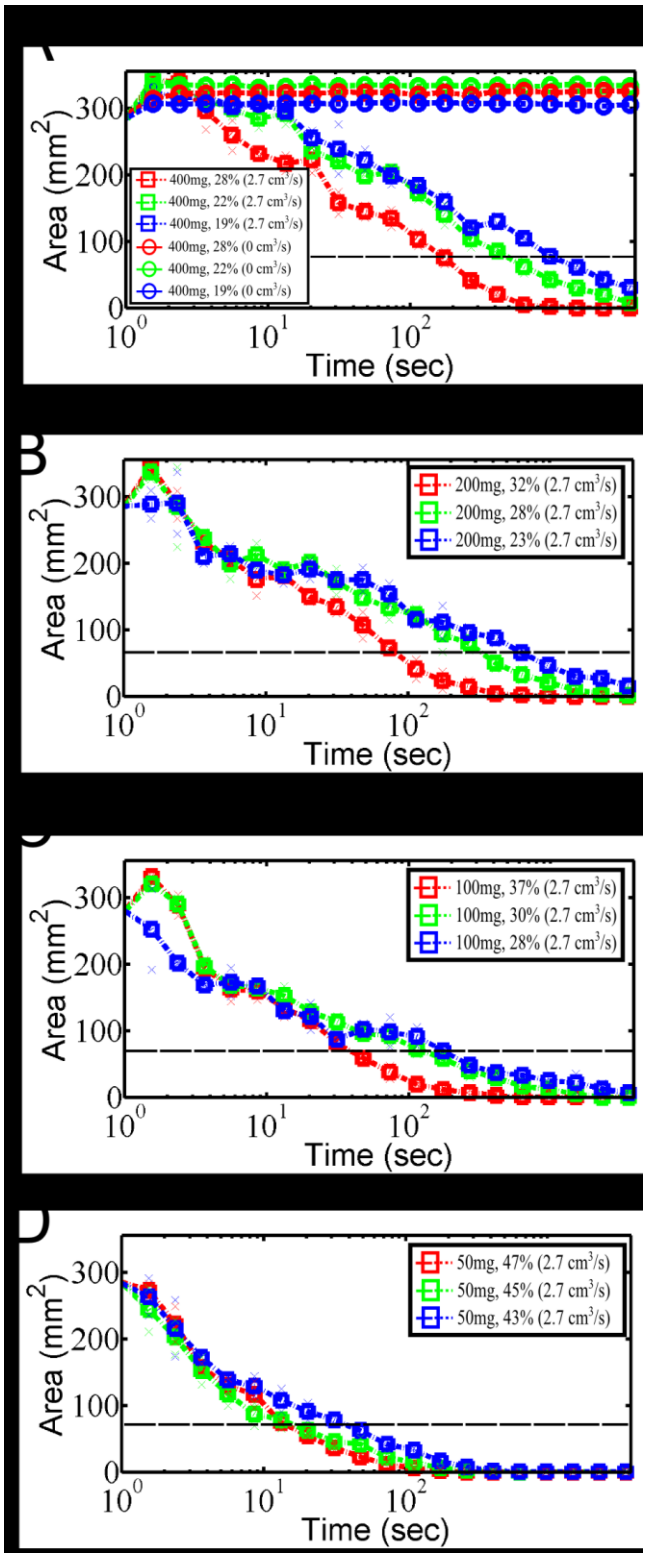

Figure 6: The plot in logarithmic scale illustrates how bubble-agitated water enhanced the size reduction of thin sheets depending on the quantity of powdered MCC: (a) 400 mg, (b)

200 mg, (c) 100 mg, and (d) 50mg. The dashed lines represent the area when the substrates became the quarter of the initial size. All the substrates experienced swelling when water penetrated the voids and weakened the internal bonding of compacted thin sheets. However, the data set with 400 mg of MCC show this occurrence. The bubbles completely disintegrated the group of thin sheets which have degrees of porosity above 28% (i.e., Combinations 1 through 6, and 9). The bubbly flow disintegrated 98%, 97%, 95%, and 89 % of the transient substrates compacted with Combinations 7, 8, 11 and 12.

collision to occur between the bubbles and the thin sheet compared to the rest of 55 minutes. There was a correlation between the porosity, which determined the hardness of the substrates, and the rate of the disintegration of the substrates in the bubbly flow. The bubbles disintegrated entire substrates fabricated with Combinations 1 through 7, and 10 within 1 hour. However, 2.4%, 2.6%, 5.5% and 11% of residues remained on the mesh screen for the Combination 6, 9, 11, and 12, respectively.

By using fundamental parameters that influenced the rate of size reduction of a substrate, we derived three sets of non-dimensional parameters. The use of constant values for a volumetric flow rate, the area of thin sheets, and a theoretical density for powdered MCC facilitated the creation of the plot that visualized the relationship among the non-dimensional parameters. The elapsed time depended on the properties of a substrate and the bubbly flow. We treated R as the time required for the size reduction of substrate that dominated the rate of disintegration and assume that

$$\mathrm{R} = \mathrm{f}\,(W_1, W_2, W_3, W_4, W_5), \tag{10}$$

where W_1= Q, the speed of bubbly flow, W_2= h, the thickness of transient substrate, W_3= ρ, the density of MCC, W_4= m, the amount of powder used for pressurized compression, W_5=A, the area of the substrate, and R=t, the time needed to be quarter size of original substrate. The quantities involved three mechanical fundamental dimensions M, L, and T (i.e., mass, length, and time). In the units we adopted in the previous step, the primary dimensions of the quantities composed of the independent dimensions: [Q] =L^3T^{-1}, [h] =L, [ρ] =ML^{-3}, [m] =M, [A] =L^2, and [t] =T. We reduced the total number of the dimensional parameters by solving the dimensional equations to obtain three non-

dimensional Π groups: $\pi_1 = \frac{Q*t}{h^3}$, $\pi_2 = \frac{\rho*h^3}{m}$, and $\pi_3 = \frac{A}{h^2}$. By substituting third dimensionless parameter for the variable in the π_2, then we set out the function:

$$\pi_1 = f(\pi_2), \tag{11}$$

or filling in the Π-terms gives:

$$\frac{Q*t}{A^{1.5}} = f\left(\frac{\rho* h^3}{m}\right), \tag{12}$$

The first non-dimensional parameter, π_1 included the variables related to the disintegrating test. Within the confines of the dimension of a thin sheet, we expect that less time will be required for the disintegration when an air pump provides a higher speed of bubbles, whereas the substrates with larger area will take longer time to disintegrate given a specific flow rate. Referring the propensity of a thin sheet depended on the quantity of a powder used for the pressurized compaction and the compaction pressure, π_2 accounted for the property of a compacted MCC. As a larger amount of pure powdered MCC was used for compression at the given compressive pressure, the thickness is increased cubically so that π_2 is extremely sensitive to the thickness of substrate. In addition, if we use the same amount of a powder consisting of MCC and lactose powder, the thickness of a compacted pellet of the binary mixture will be changed relying on the weighted fraction and the densities of two components.

As shown in Figure 7, the correlation of two non-dimensional parameters enabled the anticipation of the proclivity of the rate of disintegration of the substrate and might be useful for predicting outcomes from future experiments. According to the log-log plot for the Buckingham Pi Theorem, the amount of powdered MCC and the resulting thickness

distinguished the time needed to reduce the area of the substrates under the constant speed of bubbles as the porosity was inversely proportional to the density of the compacted MCC. For example, the substrate compacted with Combination 1, which had the highest porosity among 12 combinations, took the shortest time in the disintegration compared to the other combinations. The applied compaction pressure also influenced on the hardness of substrate, a higher compressive pressure strengthened the internal bonding of compacted MCC causing a slower size reduction, nevertheless, involved the same ratio of the pore structure. Based on the numeric data from the disintegrating test, less time was required to disintegrate the substrate with a higher degree of porosity, which had the consistency of the physical interpretation of the rate of disintegration of the transient substrate.

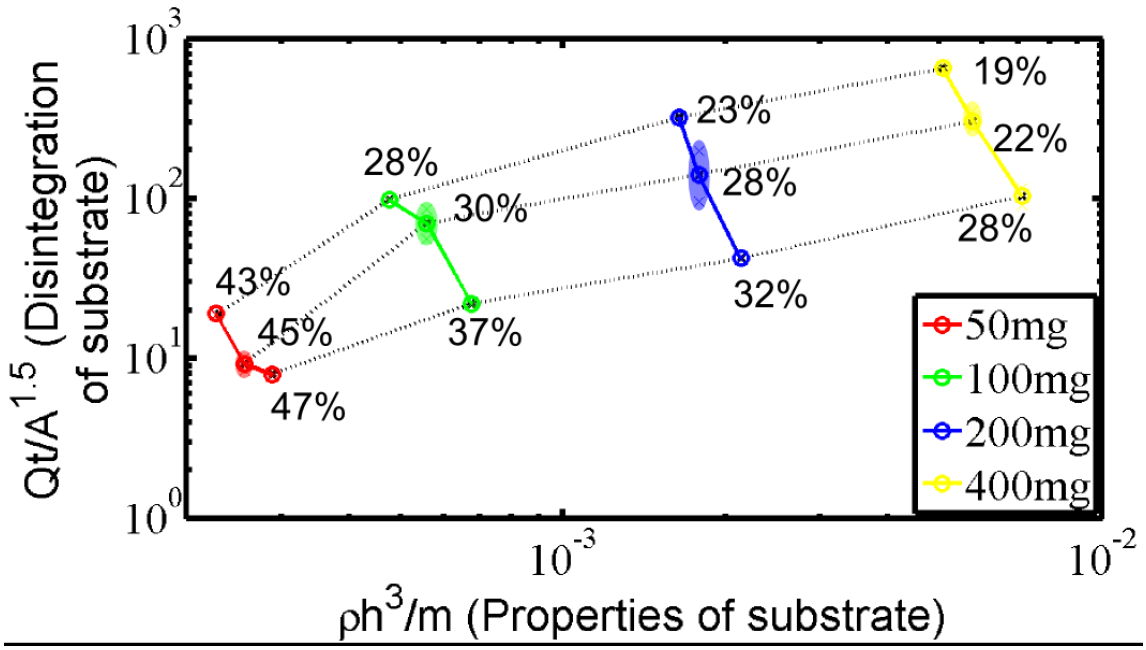

Figure 7: The Buckingham Pi Theorem supports the significance of the porosity in the rate of size reduction using the relationship between two dimensionless parameters. The porosity can be an index to predict the speed of disintegration without the experimental data. The solid lines connect the group of thin sheets which has equal quantity of powdered MCC and the dashed lines tie with the combinations compacted at the same compressive pressure. When comparing porosity values, Combination 1 includes the most porous structures among the 12 combinations. It has the fastest speed of disintegration which reduces to be a quarter of the initial size. The substrates compacted at a higher compressive pressure result in a lower porosity with a slower rate of disintegration.

3.2 Performance of Touch Sensor and Digital Keypad

To measure the insulating property of compacted MCC, impedance analyzer (HP4192A) was used to measure the changes in impedance and capacitance of compacted MCC at varying frequencies between 5 Hz and 13,000 kHz. Combinations 4 and 8, which varied in the thickness of the substrates, resulted in dielectric constant measurements ranging from 1.0 to 2.4. We demonstrated the functionality of a button by using the LCR meter (B&K Precision). Upon touching the button, the capacitance increased from 17 pF to 5.5μF responding to touch. Ten corresponding capacitive buttons were arranged in a block to create a digital keypad for the application. A printed circuit board (PCB) physically integrated ten electrical touch sensors with the surface-mounted wirings. The wirings were aggregated with an Arduino-based system via 11 pins block terminal, soldered on PCB. We designed a single layered PCB (OSH Park) with dimension of 8 cm width by 11 cm height as shown in figure 8a. The PCB had ten with 12 mm a diameter holes for each button that allowed the bubbles flow through the buttons attached on the board. Conductive ink was used to form a trail between the buttons and the PCB. The touch sensors were further connected to the pad of each assigned wiring on the surface of the PCB to transmit the electrical signal when the finger touched the touch sensors. To distribute the electrical signals to each corresponding buttons, we used a demultiplexer chip (TI CD4067 BE 1:16), a 16-bit microcontroller, which sufficiently forwarded one electrical signal to 10 individual buttons. The demux took single input from touching, then switched and transmitted the binary information to activate the output on the unique channel while others remained inactive. As a result, the connection of the demux with the RC circuit and an op-amp on the breadboard equalized the output to each button on the digital keypad.

On the other breadboard, we employed ten LEDs connecting to each digital input pin on the Arduino UNO to response the touching as seen in Figure 8b. Each button has interdigitated eletrodes with individual conductive trace to form an active electrode, while all the buttons share the same electrical ground. The produced measurable changes in capacitance triggered the corresponding LED when the finger bridged the electrical traces on individual capacitive button. Simultaneous touching of multiple touch sensors caused lighting multiple LEDs.

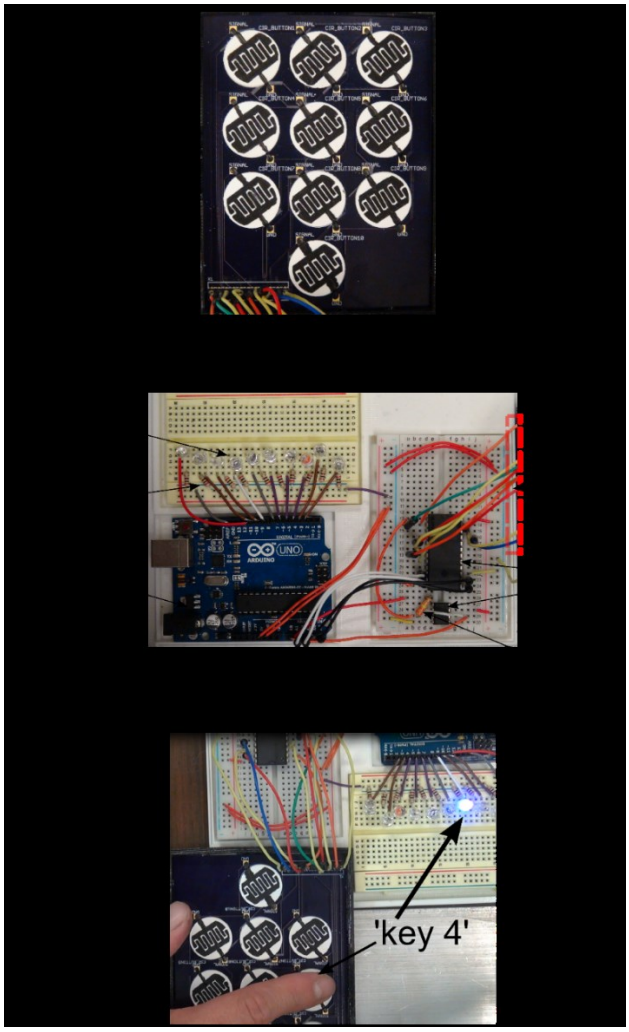

Figure 8: A digital keypad with capacitive buttons integrated with a conventional PCB. (a) Photo of a keypad comprising ten touch sensors on the PCB. With the dimension 8 cm width and 11 cm height, the single layered PCB has ten holes, composed of three rows and three columns numbers of "1" through "9", and another extra row has the place for the number of "0". An 11-pin block terminal aggregates the surface wirings on the PCB to transmit the measurable changes in capacitance to the Arduino-based system. (b) Photo of all the electrical components connected on the breadboard and Arduino UNO. (c) Each touch sensor addressed an individual LED. The corresponding LED lit up when the finger touched button "4".

4. Conclusions

The use of powdered MCC exhibited the possibility that will open up new opportunities in the field of transient touch sensors. The pressurized compaction of pure MCC varied the thicknesses of thin sheets containing the different degree of pore structures that related to the transience of substrates. The plots for the changing area of thin sheets as a function of time in the logarithmic scale accounted for the efficacy of the bubble-agitated water which disintegrated the compacted substrates much more quickly than sheets left in quiescent water. The Buckingham Pi Theorem provided the information associated with the porosity and the rate of size reduction from the bubbly flow based on the numerical data obtained from the disintegrating experiment. The technique for the stencil-patterning of electrodes granted a conductive property to thin sheets in the fabrication of capacitive button. The touch sensor triggered a reaction with an Arduino-based system that activated the LED when the finger bridged the electrical traces. By integrating ten touch sensors with the conventional electronic device, a digital keypad served as a demonstration.

In the future, thin sheets with binary mixtures consisting of MCC and other components, such as powdered lactose or disintegrant, will vary the rate of the disintegration of the substrate including the pore structures in the bubble-agitated water. The speed of bubbles controlled by the concentration of chemical reactions may enhance the efficiency of the size reduction of a transient substrate. In addition, the mixture potentially enable the fabrication of a flexible and degradable electronic device.

Appendix A: Supplementary Figures

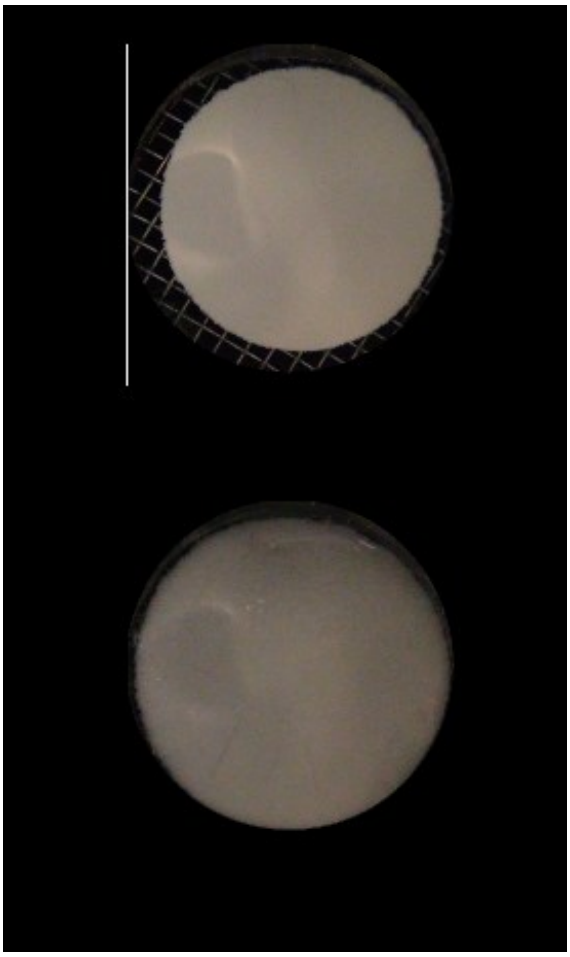

Supplementary Fig. 1: The swelling effect of compacted thin sheet with combination 6 (i.e., 100 mg of powdered MCC compacted at 90 MPa). When the substrate was immersed in the water, the water soaked into the porous regime of the substrate, and then reacted with the amorphous region of compacted MCC. The swelling can lead to cracks on the surface of a substrate regardless of the quantities of MCC used for compaction. The comparison of the area of the substrate based on the diameter was obtained from the object analysis in MATLAB Image Processing Toolbox to verify the swelling effect of water.

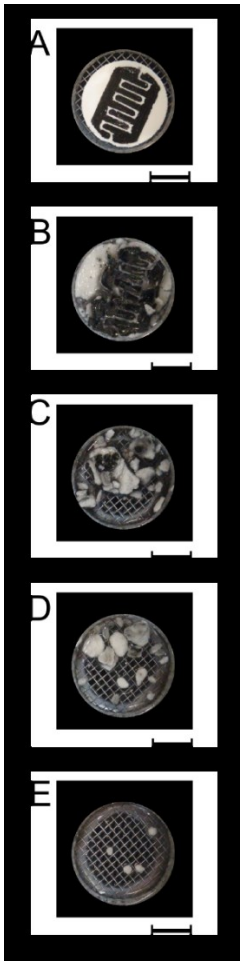

Supplementary Fig. 2: Images of the changing area of a button of Combination 7 (i.e. 200 mg of powdered MCC compacted at 90 MPa). (a) Before introducing the bubble-agitated water, it was possible to observe the E-shaped electrode. (b) 3.3 seconds after introducing the bubbles, a button swelled and became disfigured as the substrate absorbed the water. (c) After 20 seconds, the bubbles broke the button apart into small pieces, becoming unrecognizable. (d) 110 seconds later, water dissolved the majority of conductive ink on the substrate. (e) Only a few pieces of residue without conductive material remained on the mesh screen over 1 hour. When comparing the button to the substrate fabricated with same condition, the area of leftover was approximately 2.2 times as large as that of Combination 7.

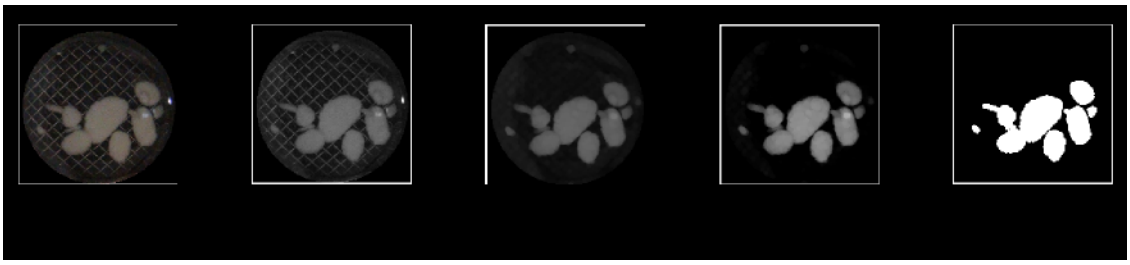

Supplementary Fig. 3: The step by step of image processing. (a) The size of the original image was befitted to focus on the desired area of the substrate ("imcrop"). (b)The cropped image was converted to gray scale for further morphological enhancement and analysis ("rgb2gray"). (c) The limitation of the luminance removed the background characteristic such as the mesh screen and reflection of water to facilitate the dilation of fragments on the images ("imopen"). (d) By selecting the brightness within the specified ranges and eroding the selected pixels to neighboring pixels, the areas of post-processed images were approximately same as raw images ("imadjust"). (e) To calculate the numerical value of the area of the substrate, the adjusted image was converted into a black and white image ("im2bw). In the final step, we converted the unit of collected data into the metric system and then plotted the calculated area as a function of the semi-log scale of time.

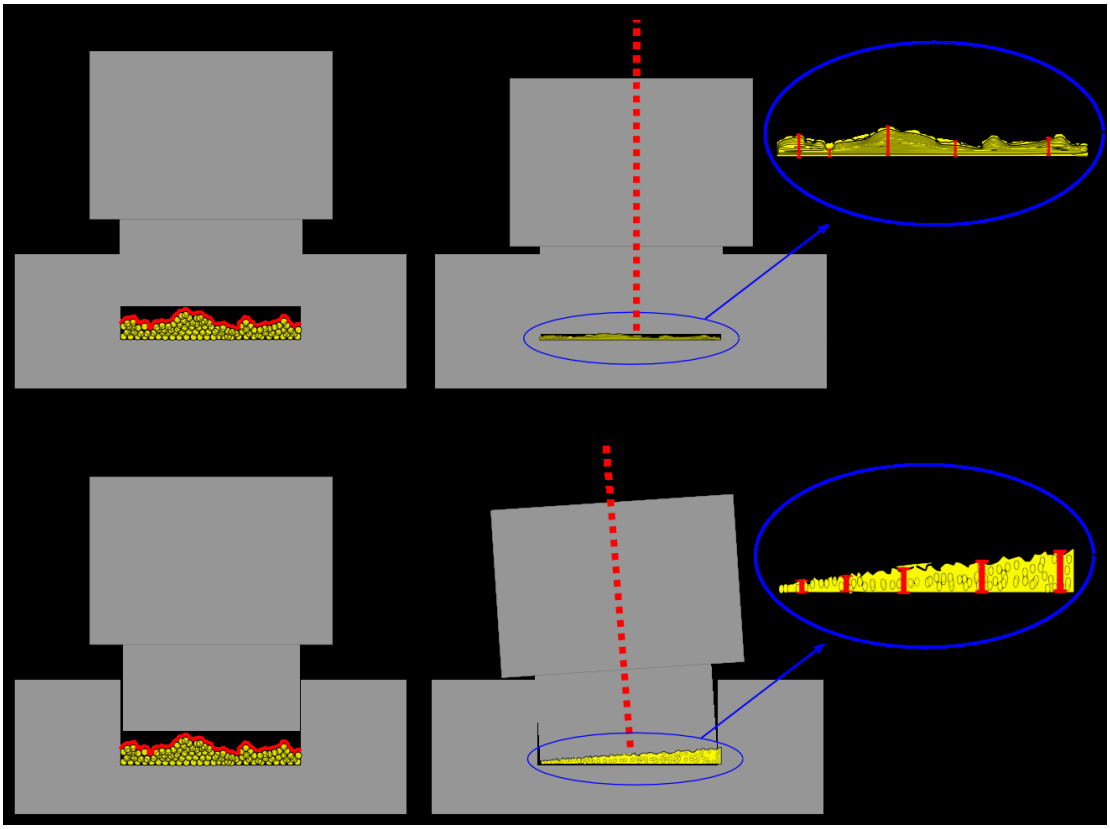

Supplementary Fig. 4: Two possible reasons for the difference in the ideal porosity and the actual porosity may be due to manufacturing imperfections: the uneven thickness of a thin sheet and misalignment of punch. (a) When the powdered MCC was randomly distributed throughout the die cavity, the flat-face punch compressed the protruding particles. Hence, the resulting thicknesses were uneven, potentially, the degrees of porosity were not linearly proportional to the quantity of powdered MCC. (b) The misalignment of the flat-face punch during the pressurized compaction caused the gradient on the substrate.

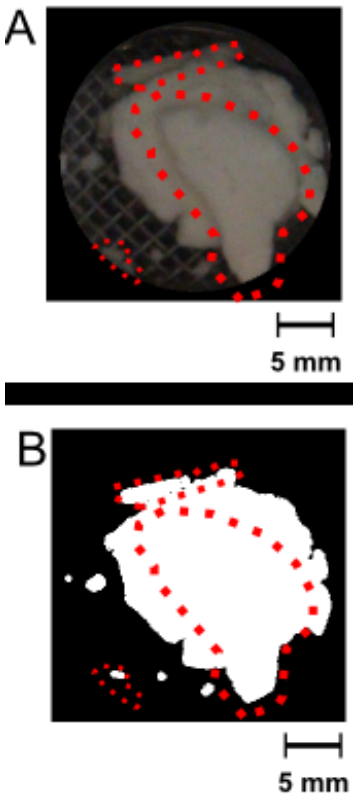

Supplementary Fig. 5: The example case of errors caused from object analysis in the 2D Image Processing. This example illustrates three types of error: Merging of two particles in layers, in adjacent placement, and missing the particles due to the intensity of luminance. When the particle was placed above the other particle or adjacent to neighboring particles, 2D image processing recognized them as a large chunky particle. The limitation of the intensity of light to eliminate background characteristic also caused the error. By analyzing a total 720 images at once with same pixel selection, the post-processed images omitted the area of particles.

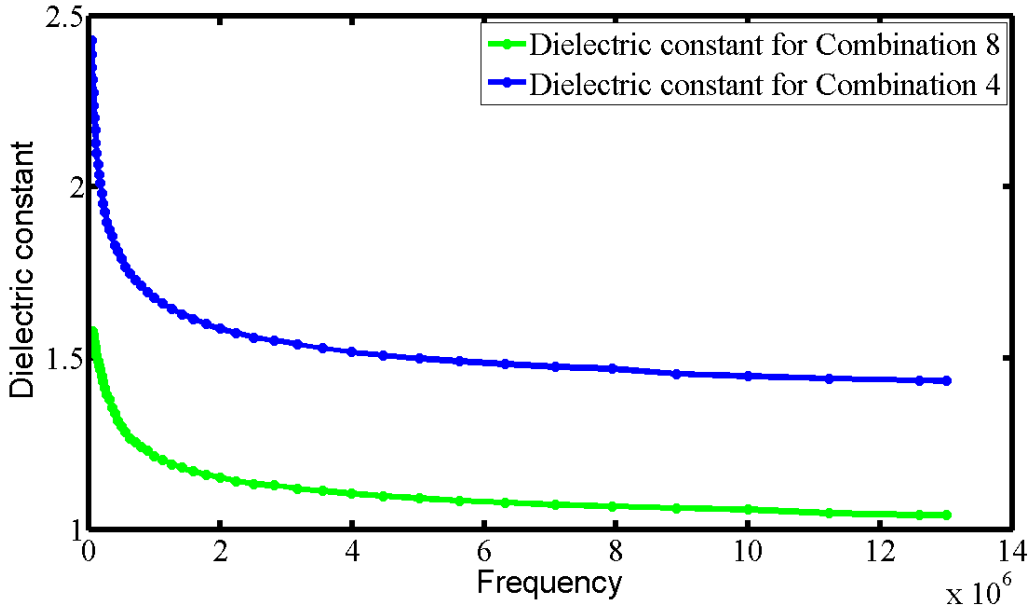

Supplementary Fig. 6: The dielectric constant of compacted thin sheets with Combinations 4 and 8. The resulting dielectric constant are lower than 2.5 which means the compacted thin sheets have insulating property.

Appendix B: Supplementary Table

Mass (mg)	Pressure (MPa)	Thickness (μm)		Porosity (%)	Size reduction of wafer (time to completely disintegrated)
		0 seconds	Relaxation (2 Hours later)		
50	45 (Comb.1)	205	210	47	100% (4.8 mins)
	90 (Comb.5)	200	200	45	100% (11 mins)
	135 (Comb.9)	190	190	43	100% (16 mins)
100	45 (Comb.2)	330	350	37	100% (10 mins)
	90 (Comb.6)	310	330	30	100% (38 mins)
	135 (Comb.10)	300	305	28	98%
200	45 (Comb.3)	600	640	32	100% (21 mins)
	90 (Comb.7)	560	610	28	99%
	135 (Comb.11)	520	570	23	95%
400	45 (Comb.4)	1150	1210	28	100% (25 mins)
	90 (Comb.8)	1070	1130	22	97%
	135 (Comb.12)	1010	1080	19	89%

Supplementary Table: Thicknesses of thin sheets and their corresponding porosities along with 12 combinations of pressurized compaction. The thickness is proportional to the amount of powdered MCC used for direct compression while inversely proportional to the pressure and porosity.

Appendix C: List of supplementary Movies

Supplementary Movie 1: Bubble-agitated water with the volumetric flow rate of 2.7 $cm^3/_{sec}$ (i.e., 0.08 mg/sec).

Supplementary Movie 2: The swelling of Combination 7 (200mg of powdered MCC compacted at 90 MPa) in quiescent water.

Supplementary Movie 3: Disintegration of Combination 7 in bubbly flow.

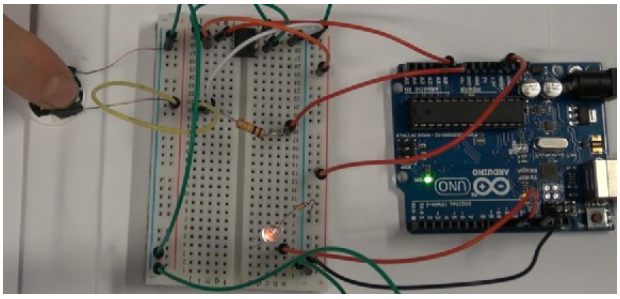

Supplementary Movie 4: The performance of a single button.

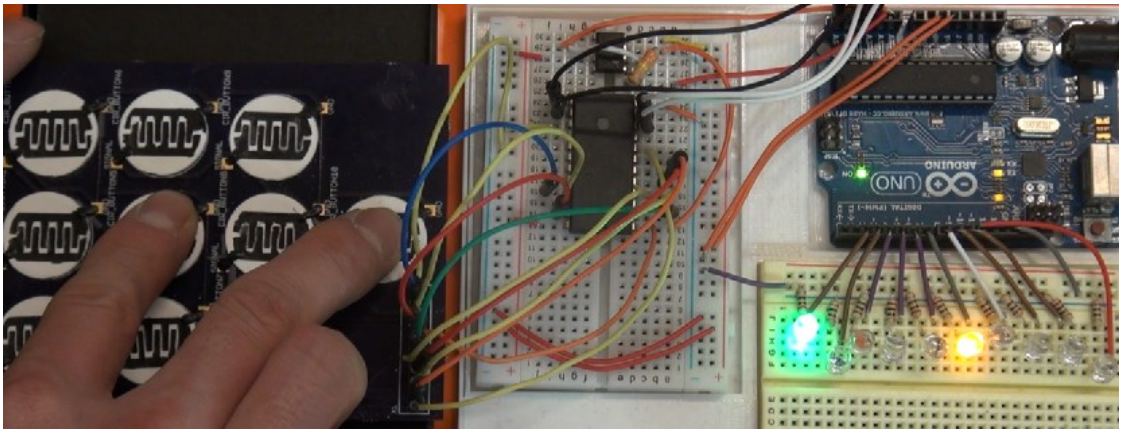

Supplementary Movie 5: The performance of ten digital key pad.

Supplementary Movie 6: Bubble-agitated water with an air pressure of 10 psi to disintegrate keypad.

Supplementary Movie 7: A keypad made with buttons of Combination 7 (i.e., 200 mg and 90 MPa) in the quiescent water.

Supplementary Movie 8: Disintegration of keypad made with buttons of Combination 7 (i.e., 200mg and 90 MPa) in bubbly flow at the air pressure of 10 psi.

Appendix D: MATLAB Code

MATLAB code for acquiring the area changing of a thin sheet disintegrated in the bubble-agitated water with a volumetric flow rate of $2.7^{cm^3}/_{sec}$

(The code below is written the size reduction for a group of transient substrates that compacted with 400 mg, but the code for the other masses and pressures are similar)

```
%% This MATLAB script was used to object analysis.
%  The transient substrate was compacted with 400 mg under three
pressures (45, 90, and 135 MPa).
%  Total 180 images includes 120 images in bubble-agitated water and 60
images in quescient water.

%% Loading the type of 'JPEG' images and setup the reference size for
the cropping.
clear all; close all; clc;
D=dir('*.jpg');
imcell=cell(1,numel(D));
areatab=[];
widthx=800; heighty=800;

%% Find the location of the cropping in circular shape in each set of
images.

factorx1=1125; factory1=1075;
factorr1=0.58*sqrt(factorx1^2+factory1^2);
circle_1_1=450; circle_2_1=425;%58 %400mg 90MPa
factorx2=1000; factory2=1025;
factorr2=0.60*sqrt(factorx2^2+factory2^2);
circle_1_2=450; circle_2_2=425;%60 %400mg 135MPa
factorx3=1500; factory3=950; factorr3=0.51*sqrt(factorx3^2+factory3^2);
circle_1_3=450; circle_2_3=425;%51 %400mg 90MPa
factorx4=1050; factory4=1025;
factorr4=0.61*sqrt(factorx4^2+factory4^2);
circle_1_4=450; circle_2_4=425;%61 %400mg 135MPa
factorx5=700; factory5=1050; factorr5=0.72*sqrt(factorx5^2+factory5^2);
circle_1_5=450; circle_2_5=425;%72 %400mg 45MPa
factorx6=700; factory6=900; factorr6=0.76*sqrt(factorx6^2+factory6^2);
circle_1_6=450; circle_2_6=425;%73 %400mg 45MPa
factorx7=200; factory7=900; factorr7=1.0*sqrt(factorx7^2+factory7^2);
circle_1_7=450; circle_2_7=425;%60 %400mg 135MPa (quiescence)
factorx8=700; factory8=950; factorr8=0.83*sqrt(factorx8^2+factory8^2);
circle_1_8=450; circle_2_8=425;%65 %400mg 90MPa (quiescence)
factorx9=0; factory9=850; factorr9=1.05*sqrt(factorx9^2+factory9^2);
circle_1_9=450; circle_2_9=425;%65 %400mg 45MPa (quiescence)

%% For-loop of the 2D image processing includes cropping the images to
get the desired area,
% pixel selection, contrast enhancement, and region properties
```

```
for i=1:180

y=imread(D(i).name);
x_1=size(y);
cenrows=x_1(1,1)/2;
cencols=x_1(1,2)/2;
if i>=1 && i<=20
z=imcrop(y,[ cenrows+factorx1,cencols-1500-
factory1,1070+widthx,heighty+1070]); size_z=size(z);
    ci=[500+circle_1_1,520+circle_2_1,factorr1];
else if i>=21 && i<=40
     z=imcrop(y,[ cenrows+factorx2,cencols-1500-
factory2,1070+widthx,heighty+1070]); size_z=size(z);
     ci=[500+circle_1_2,520+circle_2_2,factorr2];
else if i>=41 && i<=60
     z=imcrop(y,[ cenrows+factorx3,cencols-1500-
factory3,1070+widthx,heighty+1070]); size_z=size(z);
     ci=[500+circle_1_3,520+circle_2_3,factorr3];
else if i>=61 && i<=80
     z=imcrop(y,[ cenrows+factorx4,cencols-1500-
factory4,1070+widthx,heighty+1070]); size_z=size(z);
     ci=[500+circle_1_4,520+circle_2_4,factorr4];
else if i>=81 && i<=100
     z=imcrop(y,[ cenrows+factorx5,cencols-1500-
factory5,1070+widthx,heighty+1070]); size_z=size(z);
     ci=[500+circle_1_5,520+circle_2_5,factorr5];
else if i>=101 && i<=120
     z=imcrop(y,[ cenrows+factorx6,cencols-1500-
factory6,1070+widthx,heighty+1070]); size_z=size(z);
     ci=[500+circle_1_6,520+circle_2_6,factorr6];
else if i>=121 && i<=140
    z=imcrop(y,[ cenrows+factorx7,cencols-1500-
factory7,1070+widthx,heighty+1070]); size_z=size(z);
    ci=[500+circle_1_7,520+circle_2_7,factorr7];
else if i>=141 && i<=160
    z=imcrop(y,[ cenrows+factorx8,cencols-1500-
factory8,1070+widthx,heighty+1070]); size_z=size(z);
    ci=[500+circle_1_8,520+circle_2_8,factorr8];
else if i>=161 && i<=180
    z=imcrop(y,[ cenrows+factorx9,cencols-1500-
factory9,1070+widthx,heighty+1070]); size_z=size(z);
    ci=[500+circle_1_9,520+circle_2_9,factorr9];
    end
    end
    end
    end
    end
    end
    end
    end

end
   [xx,yy]=ndgrid((1:size_z(1))-ci(1),(1:size_z(2))-ci(2));
    mask=uint8((xx.^2+yy.^2)<ci(3)^2);
    z2=uint8(zeros(size(z)));
```

```
    z3(:,:,1)=z(:,:,1).*mask;
    z3(:,:,2)=z(:,:,2).*mask;
    z3(:,:,3)=z(:,:,3).*mask;
%figure; imshow(z3); %imtool(z3);
z_origin=z3;
z_gray=rgb2gray(z_origin);
z_dilated=imopen(z_gray,strel('disk',25));
z_adjust=imadjust(z_dilated,[0.07,0.60],[],1.2);
z_sharpened=imsharpen(z_adjust);
temp=zeros(1070+widthx,1070+heighty,3);
for n=1:1070+widthx
    for m=1:1070+heighty
        if z_sharpened(n,m)>=50
            temp(n,m,1:3)=255;
            end
    end

end
cropbs=im2bw(temp);
se=strel('disk',3);
cropbw=imerode(cropbs,se);
areatab=[areatab;bwarea(cropbw)];
end

%% Unit conversion from pixel to metric system (mm) and assign the x,y
values

areatab1=areatab(1:20); px2me1=1712.21/21;
areatab2=areatab(21:40); px2me2=1732.08/21;
areatab3=areatab(41:60); px2me3=1748.27/21;
areatab4=areatab(61:80); px2me4=1741.68/21;
areatab5=areatab(81:100); px2me5=1746.68/21;
areatab6=areatab(101:120); px2me6=1736.68/21;
areatab7=areatab(121:140); px2me7=1860.91/21;
areatab8=areatab(141:160); px2me8=1880.52/21;
areatab9=areatab(161:180); px2me9=1880.55/21;
matab1= areatab1/px2me1^2;matab2= areatab2/px2me2^2; matab3=
areatab3/px2me3^2;
matab4= areatab4/px2me4^2; matab5= areatab5/px2me5^2; matab6=
areatab6/px2me6^2;
matab7= areatab7/px2me7^2; matab8= areatab8/px2me8^2; matab9=
areatab9/px2me9^2;
h1=matab1'; h2=matab2'; h3=matab3'; h4=matab4'; h5=matab5';h6=matab6';
h7=matab7'; h8=matab8'; h9=matab9';
% Average the thickness along with the pressure
M1=[h1;h3]; M2=[h2;h4]; M3=[h5;h6];
at_1=mean(M1); at_2=mean(M2); at_3=mean(M3);
% Assign the time in logarithmic scale
x=logspace(0,3.55,20); timetab_1=x';

%% Create the semi-logarithmic plot to view the tendency of the
disintegration of compacted thin sheets
 figure(501);
 hLine1=semilogx(timetab_1,at_3,'-.rs','MarkerSize',20,'LineWidth',8);
 hold all;
 hLine7=semilogx(timetab_1,h5,'rx','MarkerSize',15);
```

```
 hLine8=semilogx(timetab_1,h6,'rx','MarkerSize',15);
 hLine2=semilogx(timetab_1,at_1,'-.gs','MarkerSize',20,'LineWidth',8);
 hLine9=semilogx(timetab_1,h1,'gx','MarkerSize',15);
 hLine10=semilogx(timetab_1,h3,'gx','MarkerSize',15);
 hLine3=semilogx(timetab_1,at_2,'-.bs','MarkerSize',20,'LineWidth',8);
 hLine11=semilogx(timetab_1,h2,'bx','MarkerSize',15);
 hLine12=semilogx(timetab_1,h4,'bx','MarkerSize',15);
 hLine4=semilogx(timetab_1,matab7,'-go','MarkerSize',20,'LineWidth',8);
 hLine5=semilogx(timetab_1,matab8,'-ro','MarkerSize',20,'LineWidth',8);
 hLine6=semilogx(timetab_1,matab9,'-bo','MarkerSize',20,'LineWidth',8);
 hold off;
  axis([0.0 3.85*10^3 0 355])
legend([hLine1,hLine2,hLine3,hLine4,hLine5,hLine6],'400mg, 23%
(2.7cm^3/s)','400mg, 17% (2.7cm^3/s)','400mg, 11% (2.7cm^3/s)','400mg,
23% (0cm^3/s)',...
    '400mg, 17% (0cm^3/s)','400mg, 11%
(0cm^3/s)','Location','southwest','Orientation','vertical');
xlabel ('Time (sec)','FontSize',45);
ylabel ('Area (mm^2)','FontSize',45);
set(gca,'LineWidth',5,'FontSize',45,'FontWeight','normal','FontName','T
imes')

%% Save the set of data in excel
filename_1='Total400mg.mat'; save(filename_1);
A=[matab1;matab2;matab3;matab4;matab5;matab6]; B=[at_3;at_1;at_2];
filename_2='Total400mg.xlsx'; xlswrite(filename_2,A);
filename_3='Avg400mg.xlsx';xlswrite(filename_3,B);
```

Appendix E: Arduino Code

Assign each LED to a button and estimate the capacitance by calculating the time required

the button takes to charge

```
#define Output A1
#define Input A0
#define LED0 11
#define LED1 10
#define LED2 9
#define LED3 8
#define LED4 7
#define LED5 6
#define LED6 5
#define LED7 4
#define LED8 3
#define LED9 2
#define MultiplexA A2
#define MultiplexB A3
#define MultiplexC A4
#define MultiplexD A5

unsigned long StartTime;
unsigned long ElapsedTime1;
unsigned long ElapsedTime2;
unsigned long ElapsedTime3;
unsigned long ElapsedTime4;
unsigned long ElapsedTime5;
unsigned long ElapsedTime6;
unsigned long ElapsedTime7;
unsigned long ElapsedTime8;
unsigned long ElapsedTime9;
unsigned long ElapsedTime10;
unsigned long TotalStartTime;
const int NumReadings=30;
const int SkipCountsForSmoothing=5;
int AverageNow=0;
long int Counter=0;

int Threshold1=45;
int Threshold2=45;
int Threshold3=45;
int Threshold4=45;
int Threshold5=45;
```

```
int Threshold6=45;
int Threshold7=45;
int Threshold8=45;
int Threshold9=45;
int Threshold10=45;

const float ThresholdFactor=1.02;
int Thresholds1[NumReadings];
int Thresholds2[NumReadings];
int Thresholds3[NumReadings];
int Thresholds4[NumReadings];
int Thresholds5[NumReadings];
int Thresholds6[NumReadings];
int Thresholds7[NumReadings];
int Thresholds8[NumReadings];
int Thresholds9[NumReadings];
int Thresholds10[NumReadings];

int ThresholdsTotal1=NumReadings*Threshold1;
int ThresholdsTotal2=NumReadings*Threshold2;
int ThresholdsTotal3=NumReadings*Threshold3;
int ThresholdsTotal4=NumReadings*Threshold4;
int ThresholdsTotal5=NumReadings*Threshold5;
int ThresholdsTotal6=NumReadings*Threshold6;
int ThresholdsTotal7=NumReadings*Threshold7;
int ThresholdsTotal8=NumReadings*Threshold8;
int ThresholdsTotal9=NumReadings*Threshold9;
int ThresholdsTotal10=NumReadings*Threshold10;

int Index1=0;
int Index2=0;
int Index3=0;
int Index4=0;
int Index5=0;
int Index6=0;
int Index7=0;
int Index8=0;
int Index9=0;
int Index10=0;

void setup()
{
  pinMode(Output, OUTPUT);
  pinMode(Input, INPUT);
  pinMode(LED1, OUTPUT);
  pinMode(LED2, OUTPUT);
```

```
  pinMode(LED3, OUTPUT);
  pinMode(LED4, OUTPUT);
  pinMode(LED5, OUTPUT);
  pinMode(LED6, OUTPUT);
  pinMode(LED7, OUTPUT);
  pinMode(LED8, OUTPUT);
  pinMode(LED9, OUTPUT);
  pinMode(LED0, OUTPUT);
  pinMode(MultiplexA, OUTPUT);
  pinMode(MultiplexB, OUTPUT);
  pinMode(MultiplexC, OUTPUT);
  pinMode(MultiplexD, OUTPUT);
  digitalWrite(MultiplexA, LOW);
  digitalWrite(MultiplexB, LOW);
  digitalWrite(MultiplexC, LOW);
  digitalWrite(MultiplexD, LOW);
  digitalWrite(LED1,LOW);
  digitalWrite(LED2,LOW);
  digitalWrite(LED3,LOW);
  digitalWrite(LED4,LOW);
  digitalWrite(LED5,LOW);
  digitalWrite(LED6,LOW);
  digitalWrite(LED7,LOW);
  digitalWrite(LED8,LOW);
  digitalWrite(LED9,LOW);
  digitalWrite(LED0,LOW);

  for(int ThisReading=0; ThisReading < NumReadings; ThisReading++){
    Thresholds1[ThisReading]=Threshold1;
    Thresholds2[ThisReading]=Threshold2;
    Thresholds3[ThisReading]=Threshold3;
    Thresholds4[ThisReading]=Threshold4;
    Thresholds5[ThisReading]=Threshold5;
    Thresholds6[ThisReading]=Threshold6;
    Thresholds7[ThisReading]=Threshold7;
    Thresholds8[ThisReading]=Threshold8;
    Thresholds9[ThisReading]=Threshold9;
    Thresholds10[ThisReading]=Threshold10;
  }
  Serial.begin(9600);
  Serial.println("System for Measuring Capacitance");
  Serial.println("Time to reach 2V in microseconds");
  TotalStartTime=millis();

}
void loop()
```

```
{
 digitalWrite(MultiplexA,LOW);
 digitalWrite(MultiplexB,HIGH);
 digitalWrite(MultiplexC,LOW);
 digitalWrite(MultiplexD,HIGH);
 delay(10);
 digitalWrite(Output,HIGH);
 StartTime=micros();
 while(digitalRead(Input)<1){
 }
 ElapsedTime1=micros()-StartTime;
 digitalWrite(Output,LOW);
 delay(20);

 digitalWrite(MultiplexA,HIGH);
 digitalWrite(MultiplexB,LOW);
 digitalWrite(MultiplexC,LOW);
 digitalWrite(MultiplexD,HIGH);
 delay(10);
 digitalWrite(Output,HIGH);
 StartTime=micros();
 while(digitalRead(Input)<1){
 }
 ElapsedTime2=micros()-StartTime;
 digitalWrite(Output,LOW);
 delay(20);

 digitalWrite(MultiplexA,LOW);
 digitalWrite(MultiplexB,LOW);
 digitalWrite(MultiplexC,LOW);
 digitalWrite(MultiplexD,HIGH);
 delay(10);
 digitalWrite(Output,HIGH);
 StartTime=micros();
 while(digitalRead(Input)<1){
 }
 ElapsedTime3=micros()-StartTime;
 digitalWrite(Output,LOW);
 delay(20);

 digitalWrite(MultiplexA,HIGH);
 digitalWrite(MultiplexB,HIGH);
 digitalWrite(MultiplexC,HIGH);
 digitalWrite(MultiplexD,LOW);
 delay(10);
 digitalWrite(Output,HIGH);
```

```
StartTime=micros();
while(digitalRead(Input)<1){
}
ElapsedTime4=micros()-StartTime;
digitalWrite(Output,LOW);
delay(20);

digitalWrite(MultiplexA,LOW);
digitalWrite(MultiplexB,HIGH);
digitalWrite(MultiplexC,HIGH);
digitalWrite(MultiplexD,LOW);
delay(10);
digitalWrite(Output,HIGH);
StartTime=micros();
while(digitalRead(Input)<1){
}
ElapsedTime5=micros()-StartTime;
digitalWrite(Output,LOW);
delay(20);

digitalWrite(MultiplexA,HIGH);
digitalWrite(MultiplexB,LOW);
digitalWrite(MultiplexC,HIGH);
digitalWrite(MultiplexD,LOW);
delay(10);
digitalWrite(Output,HIGH);
StartTime=micros();
while(digitalRead(Input)<1){
}
ElapsedTime6=micros()-StartTime;
digitalWrite(Output,LOW);
delay(20);

digitalWrite(MultiplexA,LOW);
digitalWrite(MultiplexB,LOW);
digitalWrite(MultiplexC,HIGH);
digitalWrite(MultiplexD,LOW);
delay(10);
digitalWrite(Output,HIGH);
StartTime=micros();
while(digitalRead(Input)<1){
}
ElapsedTime7=micros()-StartTime;
digitalWrite(Output,LOW);
delay(20);
```

```
digitalWrite(MultiplexA,HIGH);
digitalWrite(MultiplexB,HIGH);
digitalWrite(MultiplexC,LOW);
digitalWrite(MultiplexD,LOW);
delay(10);
digitalWrite(Output,HIGH);
StartTime=micros();
while(digitalRead(Input)<1){
}
ElapsedTime8=micros()-StartTime;
digitalWrite(Output,LOW);
delay(20);

digitalWrite(MultiplexA,LOW);
digitalWrite(MultiplexB,HIGH);
digitalWrite(MultiplexC,LOW);
digitalWrite(MultiplexD,LOW);
delay(10);
digitalWrite(Output,HIGH);
StartTime=micros();
while(digitalRead(Input)<1){
}
ElapsedTime9=micros()-StartTime;
digitalWrite(Output,LOW);
delay(20);

digitalWrite(MultiplexA,HIGH);
digitalWrite(MultiplexB,LOW);
digitalWrite(MultiplexC,LOW);
digitalWrite(MultiplexD,LOW);
delay(10);
digitalWrite(Output,HIGH);
StartTime=micros();
while(digitalRead(Input)<1){
}
ElapsedTime10=micros()-StartTime;
digitalWrite(Output,LOW);
delay(20);

Serial.println("");
Serial.println(ElapsedTime1,DEC);
Serial.println(ElapsedTime2,DEC);
Serial.println(ElapsedTime3,DEC);
Serial.println(ElapsedTime4,DEC);
Serial.println(ElapsedTime5,DEC);
Serial.println(ElapsedTime6,DEC);
```

```
Serial.println(ElapsedTime7,DEC);
Serial.println(ElapsedTime8,DEC);
Serial.println(ElapsedTime9,DEC);
Serial.println(ElapsedTime10,DEC);
Serial.println("");
//AverageNow=Counter%SkipCountsForSmoothing;
if(ElapsedTime1> Threshold1*ThresholdFactor){
  digitalWrite(LED9,HIGH);
}
else{
digitalWrite(LED9,LOW);
}
if(ElapsedTime2> Threshold2*ThresholdFactor){
  digitalWrite(LED8,HIGH);
}
else{
digitalWrite(LED8,LOW);
}
if(ElapsedTime3> Threshold3*ThresholdFactor){
  digitalWrite(LED7,HIGH);
}
else{
digitalWrite(LED7,LOW);
}
if(ElapsedTime4> Threshold4*ThresholdFactor){
  digitalWrite(LED6,HIGH);
}
else{
digitalWrite(LED6,LOW);
}
if(ElapsedTime5> Threshold5*ThresholdFactor){
  digitalWrite(LED5,HIGH);
}
else{
digitalWrite(LED5,LOW);
if(ElapsedTime6> Threshold6*ThresholdFactor){
  digitalWrite(LED4,HIGH);
}
else{
digitalWrite(LED4,LOW);
}
if(ElapsedTime7> Threshold7*ThresholdFactor){
  digitalWrite(LED3,HIGH);
}
else{
digitalWrite(LED3,LOW);
```

```
  }
  if(ElapsedTime8> Threshold8*ThresholdFactor){
    digitalWrite(LED2,HIGH);
  }
  else{
  digitalWrite(LED2,LOW);
  }
  if(ElapsedTime9> Threshold9*ThresholdFactor){
    digitalWrite(LED1,HIGH);
  }
  else{
  digitalWrite(LED1,LOW);
  }
  if(ElapsedTime10> Threshold10*ThresholdFactor){
    digitalWrite(LED0,HIGH);
  }
  else{
  digitalWrite(LED0,LOW);
  }
}
}
```

References

[1] B. H. Robinson, “E-waste: An assessment of global production and environmental impacts,” *Science of The Total Environment*, vol. 408, no. 2, pp. 183–191, Dec. 2009.
[2] A. Tanaka, “Toxicity of indium arsenide, gallium arsenide, and aluminium gallium arsenide,” *Toxicology and Applied Pharmacology*, vol. 198, no. 3, pp. 405–411, Aug. 2004.
[3] M. Irimia-Vladu, E. D. G\lowacki, G. Voss, S. Bauer, and N. S. Sariciftci, “Green and biodegradable electronics,” *Materials Today*, vol. 15, no. 7, pp. 340–346, 2012.
[4] D.-H. Kim, J. Viventi, J. J. Amsden, J. Xiao, L. Vigeland, Y.-S. Kim, J. A. Blanco, B. Panilaitis, E. S. Frechette, D. Contreras, D. L. Kaplan, F. G. Omenetto, Y. Huang, K.-C. Hwang, M. R. Zakin, B. Litt, and J. A. Rogers, “Dissolvable films of silk fibroin for ultrathin conformal bio-integrated electronics,” *Nature Materials*, vol. 9, no. 6, pp. 511–517, Jun. 2010.
[5] S.-W. Hwang, H. Tao, D.-H. Kim, H. Cheng, J.-K. Song, E. Rill, M. A. Brenckle, B. Panilaitis, S. M. Won, Y.-S. Kim, Y. M. Song, K. J. Yu, A. Ameen, R. Li, Y. Su, M. Yang, D. L. Kaplan, M. R. Zakin, M. Slepian, Y. Huang, F. G. Omenetto, and J. A. Rogers, “A Physically Transient Form of Silicon Electronics,” *Science*, vol. 337, no. 6102, pp. 1640–1644, Sep. 2012.
[6] S.-W. Hwang, J.-K. Song, X. Huang, H. Cheng, S.-K. Kang, B. H. Kim, J.-H. Kim, S. Yu, Y. Huang, and J. A. Rogers, “High-Performance Biodegradable/Transient Electronics on Biodegradable Polymers,” *Advanced Materials*, vol. 26, no. 23, pp. 3905–3911, Jun. 2014.
[7] A. D. Mazzeo, W. B. Kalb, L. Chan, M. G. Killian, J.-F. Bloch, B. A. Mazzeo, and G. M. Whitesides, “Paper-Based, Capacitive Touch Pads,” *Advanced Materials*, vol. 24, no. 21, pp. 2850–2856, Jun. 2012.
[8] M. Fahlman and W. R. Salaneck, “Surfaces and interfaces in polymer-based electronics,” *Surface Science*, vol. 500, no. 1, pp. 904–922, 2002.
[9] D. Tobjörk and R. Österbacka, “Paper electronics,” *Advanced Materials*, vol. 23, no. 17, pp. 1935–1961, 2011.
[10] G. Thoorens, F. Krier, B. Leclercq, B. Carlin, and B. Evrard, “Microcrystalline cellulose, a direct compression binder in a quality by design environment—A review,” *International Journal of Pharmaceutics*, vol. 473, no. 1–2, pp. 64–72, Oct. 2014.
[11] D. McCormick, “Evolutions in direct compression,” *Pharmaceutical Technology*, vol. 17, no. 4, pp. 52–62, 2005.
[12] M. Kamba, Y. Seta, N. Takeda, T. Hamaura, A. Kusai, H. Nakane, and K. Nishimura, “Measurement of agitation force in dissolution test and mechanical destructive force in disintegration test,” *International journal of pharmaceutics*, vol. 250, no. 1, pp. 99–109, 2003.
[13] J. Rojas, “Effect of Polymorphism on the Particle and Compaction Properties of Microcrystalline Cellulose,” in *Cellulose - Medical, Pharmaceutical and Electronic Applications*, T. G. M. Van De Ven, Ed. InTech, 2013.
[14] P.-F. Sung, Y.-L. Hsieh, K. Angonese, D. Dunn, R. J. King, R. Machbitz, A. Christianson, W. J. Chappell, L. S. Taylor, and M. T. Harris, “Complex Dielectric Properties of Microcrystalline Cellulose, Anhydrous Lactose, and α-Lactose

Monohydrate Powders Using a Microwave-Based Open-Reflection Resonator Sensor," *Journal of Pharmaceutical Sciences*, vol. 100, no. 7, pp. 2920–2934, Jul. 2011.
[15] W. J. Hyun, E. B. Secor, M. C. Hersam, C. D. Frisbie, and L. F. Francis, "High-Resolution Patterning of Graphene by Screen Printing with a Silicon Stencil for Highly Flexible Printed Electronics," *Advanced Materials*, vol. 27, no. 1, pp. 109–115, Jan. 2015.
[16] Arduino. www.arduino.cc
[17] C. (Calvin) Sun, "True Density of Microcrystalline Cellulose," *Journal of Pharmaceutical Sciences*, vol. 94, no. 10, pp. 2132–2134, Oct. 2005.